Influence of Heat Transfer and Magnetic Field on a Peristaltic Transport of a Jeffrey Fluid in an Asymmetric Channel with Partial Slip

Sohail Nadeem and Safia Akram

Department of Mathematics, Quaid-i-Azam University 45320, Islamabad 44000, Pakistan

Reprint requests to S. N.; Fax: +92 92512275341; E-mail: snqau@hotmail.com

Z. Naturforsch. **65a,** 483 – 494 (2010); received March 3, 2009 / revised September 15, 2009

In the present paper, we have studied the influence of heat transfer and magnetic field on a peristaltic transport of a Jeffrey fluid in an asymmetric channel with partial slip. The complicated Jeffrey fluid equations are simplified using the long wave length and low Reynolds number assumptions. In the wave frame of reference, an exact and closed form of Adomian solution is presented. The expressions for pressure drop, pressure rise, stream function, and temperature field have been calculated. The behaviour of different physical parameters has been discussed graphically. The pumping and trapping phenomena of various wave forms (sinusoidal, multisinusoidal, square, triangular, and trapezoidal) are also studied.

Key words: Exact Solution; Adomian Solution; Partial Slip; Peristaltic Flow; Asymmetric Channel; Heat Transfer Analysis.

1. Introduction

Recently, Kothandapani and Srinivas [1] have discussed the peristaltic flow of a Jeffrey fluid in an asymmetric channel in the presence of a transverse magnetic field. They employ for the Jeffrey fluid a relatively simple linear model using time derivatives instead of convective derivatives. Their observation was that the size of trapped bolus in the Jeffrey fluid is much smaller than in the Newtonian fluid. Due to the large number of applications, the peristaltic flows for different fluids and different geometries have been discussed by a number of researchers [1 – 15]. Only a limited attention has been focused on the study of peristaltic flows in the presence of heat transfer analysis. Mention may be made to the works of [16 – 23]. No attempt has been made to discuss the slip effects on the peristaltic transport of a Jeffrey fluid in an asymmetric channel in the presence of heat transfer analysis. Therefore the aim of the present paper is to discuss the influence of heat transfer and magnetic field on a peristaltic transport of a Jeffrey fluid (non-Newtonian) with partial slip in an asymmetric channel. The exact and closed form of Adomian solutions are obtained under the assumptions of long wave length and low Reynolds number. Many existing solutions in the literature are found to be subcases of our problem. The influence of physical parameters on the pressure rise, temperature, and stream function have been studied for five types of wave forms, namely sinusoidal, multisinusoidal, square, trapezoidal, and triangular.

2. Mathematical Formulation

We consider magnotohydrodynamic (MHD) flow of an electrically conducting Jeffrey fluid in an asymmetric channel. The lower wall of the channel is maintained at temperature T_1 while the upper wall has temperature T_0. We assume that the fluid is subject to a constant transverse magnetic field $\mathbf{B}$. A very small magnetic Reynolds number is assumed and hence the induced magnetic field can be neglected. When the fluid moves into the magnetic field two major physical effects arise. The first one is that an electric field $\mathbf{E}$ is induced in the flow. We shall assume that there is no excess charge density and therefore, $\nabla\cdot\mathbf{E}=0$. Neglecting the induced magnetic field implies that $\nabla\times\mathbf{E}=0$ and therefore, the induced electric field is negligible. The second effect is dynamically in nature, i. e., a Lorentz force ($\mathbf{J}\times\mathbf{B}$), where $\mathbf{J}$ is the current density. This force acts on the fluid and modifies its motion resulting in the transfer of energy from the electromagnetic field to the fluid. In the present study, the relativistic effects are neglected and the current density $\mathbf{J}$ is given by Ohm's law as

$$\mathbf{J}=\sigma(\mathbf{V}\times\mathbf{B}).$$

Since we are considering an asymmetric channel, the channel flow is produced due to different amplitudes and phases of the peristaltic waves on the channel. A schematic diagram of the geometry of the problem under consideration is shown in Figure 1.

The geometry of the wall surface is defined as

$$\begin{aligned} Y &= H_1 = d_1 + a_1 \cos\left[\frac{2\pi}{\lambda}(X-ct)\right], \\ Y &= H_2 = -d_2 - b_1 \cos\left[\frac{2\pi}{\lambda}(X-ct)+\phi\right], \end{aligned} \tag{1}$$

where a_1 and b_1 are the amplitudes of the waves, λ is the wave length, d_1+d_2 is the width of the channel, c is the velocity of propagation, t is the time, and X is the direction of wave propagation. The phase difference ϕ varies in the range of $0 \le \phi \le \pi$, $\phi = 0$ corresponds to a symmetric channel with waves out of phase and for $\phi = \pi$ the waves are in phase, and further a_1, b_1, d_1, d_2, and ϕ satisfy the condition

$$a_1^2 + b_1^2 + 2a_1 b_1 \cos\phi \le (d_1+d_2)^2.$$

Taking into account the magnetic Lorentz force, the equations governing the flow of a Jeffrey fluid are given by

$$\begin{aligned} &\frac{\partial U}{\partial X} + \frac{\partial V}{\partial Y} = 0, \\ &\rho\left(\frac{\partial U}{\partial t} + U\frac{\partial U}{\partial X} + V\frac{\partial U}{\partial Y}\right) = \\ &\qquad -\frac{\partial P}{\partial X} + \frac{\partial}{\partial X}(S_{XX}) + \frac{\partial}{\partial Y}(S_{XY}) - \sigma B_0^2 U, \\ &\rho\left(\frac{\partial V}{\partial t} + U\frac{\partial V}{\partial X} + V\frac{\partial V}{\partial Y}\right) = \\ &\qquad -\frac{\partial P}{\partial Y} + \frac{\partial}{\partial X}(S_{YX}) + \frac{\partial}{\partial Y}(S_{YY}), \\ &C'\left[\frac{\partial T}{\partial t} + U\frac{\partial T}{\partial X} + V\frac{\partial T}{\partial Y}\right] = \frac{K'}{\rho}\nabla^2 T + \nu\Phi, \end{aligned} \tag{2}$$

where

$$\begin{aligned} \nabla^2 &= \frac{\partial^2}{\partial X^2} + \frac{\partial^2}{\partial Y^2}, \\ \Phi &= \frac{1}{1+\lambda_1}\left[1+\lambda_2\left(U\frac{\partial}{\partial X} + V\frac{\partial}{\partial Y}\right)\right] \\ &\quad \cdot \left[2\left(\frac{\partial U}{\partial X}\right)^2 + 2\left(\frac{\partial V}{\partial Y}\right)^2 + \left(\frac{\partial U}{\partial Y} + \frac{\partial V}{\partial X}\right)^2\right]. \end{aligned}$$

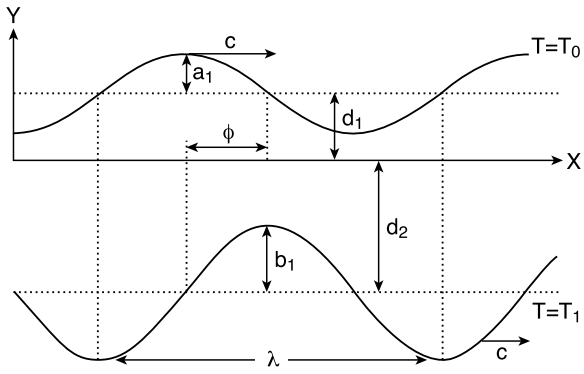

Fig. 1. Schematic diagram of a two-dimensional asymetric channel.

U, V are the velocities in X- and Y-directions in a fixed frame, ρ is the constant density, P is the pressure, ν is the kinematics viscosity, σ is the electrical conductivity, K' is the thermal conductivity, C' is the specific heat, and T is the temperature.

The constitutive equation for the extra stress tensor $\mathbf{S}$ is

$$\mathbf{S} = \frac{\mu}{1+\lambda_1}(\dot{\gamma} + \lambda_2 \ddot{\gamma}). \tag{3}$$

In above equation λ_1 is the ratio of relaxation to retardation times, $\dot{\gamma}$ the shear rate, λ_2 the retardation time, and dots denote the differentiation with respect to time.

Introducing a wave frame (x,y) moving with velocity c away from the fixed frame (X,Y) by the transformation

$$\begin{aligned} &x = X - ct, \quad y = Y, \quad u = U - c, \quad v = V, \\ &\text{and} \quad p(x) = P(X,t). \end{aligned} \tag{4}$$

Defining

$$\begin{aligned} &\bar{x} = \frac{x}{\lambda}, \quad \bar{y} = \frac{y}{d_1}, \quad \bar{u} = \frac{u}{c}, \quad \bar{v} = \frac{v}{c}, \\ &\delta = \frac{d_1}{\lambda}, \quad d = \frac{d_2}{d_1}, \quad \bar{p} = \frac{d_1^2 p}{\mu c \lambda}, \quad \bar{t} = \frac{ct}{\lambda}, \\ &h_1 = \frac{H_1}{d_1}, \quad h_2 = \frac{H_2}{d_2}, \quad a = \frac{a_1}{d_1}, \quad b = \frac{b_1}{d_1}, \\ &Re = \frac{cd_1}{\nu}, \quad \bar{\Psi} = \frac{\Psi}{cd_1}, \quad \theta = \frac{T-T_0}{T_1-T_0}, \\ &\bar{S} = \frac{Sd_1}{\mu c}, \quad Ec = \frac{c^2}{C'(T_1-T_0)}, \\ &Pr = \frac{\rho \nu C'}{K'}, \quad M = \sqrt{\frac{\sigma}{\nu}} B_0 d. \end{aligned} \tag{5}$$

Using the above non-dimensional quantities the resulting equations in terms of stream function Ψ (dropping the bars, $u=\frac{\partial\Psi}{\partial y}$, $v=-\delta\frac{\partial\Psi}{\partial x}$) can be written as

$$Re\delta[\psi_y\psi_{xy}-\psi_x\psi_{yy}]=-\frac{\partial p}{\partial x}+\delta\frac{\partial}{\partial x}(S_{xx})+\frac{\partial}{\partial y}(S_{xy})-M^2(\psi_y+1), \tag{6}$$

$$Re\delta^3[-\psi_y\psi_{xx}+\psi_x\psi_{xy}]=-\frac{\partial p}{\partial y}+\delta^2\frac{\partial}{\partial x}(S_{yx})+\delta\frac{\partial}{\partial y}(S_{yy}), \tag{7}$$

$$Re\delta[\psi_y\theta_x-\psi_x\theta_y]=\frac{1}{Pr}[\theta_{yy}+\delta^2\theta_{xx}]+\frac{Ec}{(1+\lambda_1)}\cdot\left[1+\frac{\lambda_2 c\delta}{d_1}\left(\psi_y\frac{\partial}{\partial x}-\psi_x\frac{\partial}{\partial y}\right)\right]\cdot[4\delta^2\psi_{x,y}^2+(\psi_{yy}-\delta^2\psi_{xx})^2], \tag{8}$$

where

$$S_{xx}=\frac{2\delta}{1+\lambda_1}\left[1+\frac{\lambda_2 c\delta}{d_1}\left(\psi_y\frac{\partial}{\partial x}-\psi_x\frac{\partial}{\partial y}\right)\right]\psi_{xy},$$

$$S_{xy}=\frac{1}{1+\lambda_1}\left[1+\frac{\lambda_2 c\delta}{d_1}\left(\psi_y\frac{\partial}{\partial x}-\psi_x\frac{\partial}{\partial y}\right)\right]\cdot[\psi_{yy}-\delta^2\psi_{xx}],$$

$$S_{yy}=-\frac{2\delta}{1+\lambda_1}\left[1+\frac{\lambda_2 c\delta}{d_1}\left(\psi_y\frac{\partial}{\partial x}-\psi_x\frac{\partial}{\partial y}\right)\right]\psi_{xy}.$$

The corresponding boundary conditions are

$$\begin{aligned}
&\psi=\frac{q}{2}\ \text{ at }\ y=h_1=1+a\cos 2\pi x,\\
&\psi=-\frac{q}{2}\ \text{ at }\ y=h_2=-d-b\cos(2\pi x+\phi),\\
&\frac{\partial\psi}{\partial y}+\frac{L}{(1+\lambda_1)}\frac{\partial^2\psi}{\partial y^2}=-1\ \text{ at }\ y=h_1,\\
&\frac{\partial\psi}{\partial y}-\frac{L}{(1+\lambda_1)}\frac{\partial^2\psi}{\partial y^2}=-1\ \text{ at }\ y=h_2,\\
&\theta=0\ \text{ on }\ y=h_1,\\
&\theta=1\ \text{ on }\ y=h_2,
\end{aligned} \tag{9}$$

where q is the flux in the wave frame, L represents the partial slip parameter, a, b, ϕ, and d satisfy the relation

$$a^2+b^2+2ab\cos\phi\le(1+d)^2.$$

Under the assumption of long wave length $\delta\ll 1$ and low Reynolds number, (6) to (8) become

$$0=-\frac{\partial p}{\partial x}+\frac{\partial}{\partial y}\left[\frac{1}{1+\lambda_1}\frac{\partial^2\psi}{\partial y^2}\right]-M^2(\psi_y+1), \tag{10}$$

$$0=-\frac{\partial p}{\partial y}, \tag{11}$$

$$\frac{1}{Pr}\theta_{yy}+\frac{Ec}{(1+\lambda_1)}\psi_{yy}^2=0. \tag{12}$$

Elimination of the pressure from (10) and (11), yields

$$\frac{\partial^2}{\partial y^2}\left[\frac{1}{1+\lambda_1}\frac{\partial^2\psi}{\partial y^2}\right]-M^2\psi_{yy}=0, \tag{13}$$

$$\frac{1}{Pr}\theta_{yy}+\frac{Ec}{(1+\lambda_1)}\psi_{yy}^2=0. \tag{14}$$

3. Solution of the Problem

3.1. Exact Solution

The exact solution of (13) can be written as

$$\psi=F_0+F_1y+F_2\cosh\frac{y}{\sqrt{A}}+F_3\sinh\frac{y}{\sqrt{A}}, \tag{15}$$

where F_0, F_1, F_2, F_3 are functions of x:

$$\begin{aligned}
F_0&=\frac{-(h_1+h_2)\left[q+\left(\frac{qL+2A(1+\lambda_1)}{\sqrt{A}(1+\lambda_1)}\right)\tanh\left[\frac{h_1-h_2}{2\sqrt{A}}\right]\right]}{2(h_1-h_2)-2\left(\frac{L(h_2-h_1)+2A(1+\lambda_1)}{\sqrt{A}(1+\lambda_1)}\right)\tanh\left[\frac{h_1-h_2}{2\sqrt{A}}\right]},\\
F_1&=\frac{q+\left(\frac{qL+2A(1+\lambda_1)}{\sqrt{A}(1+\lambda_1)}\right)\tanh\left[\frac{h_1-h_2}{2\sqrt{A}}\right]}{(h_1-h_2)-\left(\frac{L(h_2-h_1)+2A(1+\lambda_1)}{\sqrt{A}(1+\lambda_1)}\right)\tanh\left[\frac{h_1-h_2}{2\sqrt{A}}\right]},\\
F_2&=\frac{-\sqrt{A}(q+h_1-h_2)\operatorname{sech}\left[\frac{h_1-h_2}{2\sqrt{A}}\right]\sinh\left[\frac{h_1+h_2}{2\sqrt{A}}\right]}{(h_2-h_1)+\left(\frac{L(h_2-h_1)+2A(1+\lambda_1)}{\sqrt{A}(1+\lambda_1)}\right)\tanh\left[\frac{h_1-h_2}{2\sqrt{A}}\right]},\\
F_3&=\frac{\sqrt{A}(q+h_1-h_2)\operatorname{sech}\left[\frac{h_1-h_2}{2\sqrt{A}}\right]\cosh\left[\frac{h_1+h_2}{2\sqrt{A}}\right]}{(h_2-h_1)+\left(\frac{L(h_2-h_1)+2A(1+\lambda_1)}{\sqrt{A}(1+\lambda_1)}\right)\tanh\left[\frac{h_1-h_2}{2\sqrt{A}}\right]}.
\end{aligned} \tag{16}$$

4. Solution by the Adomian Decomposition Method

In this section, the Adomian solutions will be determined for the velocity field [24–30].

According to the Adomian decomposition method, we write (13) in the operator form

$$\acute{L}_{yyyy}\psi = M^2(1+\lambda_1)\psi_{yy}. \tag{17}$$

Applying the inverse operator $\acute{L}^{-1}_{yyyy} = \int\int\int\int[\cdot]\mathrm{d}y\mathrm{d}y\,\mathrm{d}y\mathrm{d}y$, we can write (17) as

$$\psi = C_0 + C_1 y + C_2\frac{y^2}{2!} + C_3\frac{y^3}{3!} + \frac{1}{A}\acute{L}^{-1}_{yyyy}(\psi_{yy}), \tag{18}$$

where

$$\frac{1}{A} = M^2(1+\lambda_1),$$

C_0, C_1, C_2, C_3 are functions of x. Now we decompose ψ as

$$\psi = \sum_{n=0}^{\infty}\psi_n. \tag{19}$$

Substituting ψ into (18), we obtain

$$\begin{aligned}\psi &= C_0 + C_1 y + C_2\frac{y^2}{2!} + C_3\frac{y^3}{3!},\\ \psi_{n+1} &= \frac{1}{A}\int\int\int\int(\psi_n)_{yy}\mathrm{d}y\mathrm{d}y\mathrm{d}y\mathrm{d}y, \quad n\geq 0.\end{aligned} \tag{20}$$

Therefore,

$$\begin{aligned}\psi_1 &= \frac{1}{A}\left(C_2\frac{y^4}{4!} + C_3\frac{y^5}{5!}\right),\\ \psi_2 &= \frac{1}{A^2}\left(C_2\frac{y^6}{6!} + C_3\frac{y^7}{7!}\right),\\ &\vdots\\ \psi_n &= \frac{1}{A^n}\left(C_2\frac{y^{2n+2}}{(2n+2)!} + C_3\frac{y^{2n+3}}{(2n+3)!}\right), \quad n>0.\end{aligned} \tag{21}$$

According to (19), the closed form of ψ can be written as

$$\begin{aligned}\psi = C_0 + C_1 y + AC_2\left(\cosh\frac{y}{\sqrt{A}} - 1\right)\\ + A\sqrt{A}C_3\left(\sinh\frac{y}{\sqrt{A}} - \frac{y}{\sqrt{A}}\right),\end{aligned}$$

which can be put in the simplest form

$$\psi = F_0 + F_1 y + F_2\cosh\frac{y}{\sqrt{A}} + F_3\sinh\frac{y}{\sqrt{A}}. \tag{22}$$

Now the Adomian solution (22) and the exact solution (15) are exactly the same in which F_i ($i=0$ to 3) are calculated using the boundary conditions which are defined in (16).

The flux at any axial station in the fixed frame is

$$\bar{Q} = \int_{h_2}^{h_1}(u+1)\mathrm{d}y = \int_{h_2}^{h_1}u\mathrm{d}y + \int_{h_2}^{h_1}\mathrm{d}y = q + h_1 - h_2.$$

The average volume flow rate over one period ($T=\frac{\lambda}{c}$) of the peristaltic wave is defined as

$$Q = \frac{1}{T}\int_0^T\bar{Q}\mathrm{d}t = \frac{1}{T}\int_0^T(q+h_1-h_2)\mathrm{d}t = q+1+d. \tag{23}$$

The pressure gradient is obtained from the dimensionless momentum equation for the axial velocity as

$$\frac{\mathrm{d}p}{\mathrm{d}x} = \frac{1}{(1+\lambda_1)}\left[\psi_{yyy} - \frac{1}{A}\psi_y - \frac{1}{A}\right]. \tag{24}$$

Substituting the values of ψ into (24), we obtain

$$\begin{aligned}\frac{\mathrm{d}p}{\mathrm{d}x} = -(h_1-h_2+q)\left\{1 + \frac{l}{A(1+\lambda_1)}\tanh\left(\frac{h_1-h_2}{2\sqrt{A}}\right)\right\}\\ \cdot\left\{A(1+\lambda_1)\left[h_1 - h_2 - \frac{L(h_2-h_1)+2A(1+\lambda_1)}{\sqrt{A}(1+\lambda_1)}\right.\right.\\ \left.\left.\cdot\tanh\left(\frac{h_1-h_2}{2\sqrt{A}}\right)\right]\right\}^{-1}.\end{aligned} \tag{25}$$

Integrating (25) over one wavelength, we get

$$\Delta p = \int_0^1\frac{\mathrm{d}p}{\mathrm{d}x}\mathrm{d}x.$$

The axial velocity component in the fixed frame (nondimensional form) is given by

$$\begin{aligned}U(X,Y,t) = 1+\psi_y = \left[2(h_- h_2+q)\sinh\left(\frac{h_1-Y}{2\sqrt{A}}\right)\right.\\ \cdot\sinh\left(\frac{h_2-Y}{2\sqrt{A}}\right) - \left.\frac{L(h_1-h_2+q)}{\sqrt{A}(1+\lambda_1)}\sinh\left(\frac{h_1-h_2}{2\sqrt{A}}\right)\right]\\ \cdot\left[\frac{L(h_2-h_1)+2A(1+\lambda_1)}{\sqrt{A}(1+\lambda_1)}\sinh\left(\frac{h_1-h_2}{2\sqrt{A}}\right)\right.\\ \left.-(h_1-h_2)\cosh\left(\frac{h_1-h_2}{2\sqrt{A}}\right)\right]^{-1},\end{aligned} \tag{26}$$

where

$$\begin{aligned}h_1 &= 1 + a\cos[2\pi(X-t)] \text{ and}\\ h_2 &= -d - b\cos[2\pi(X-t)+\phi].\end{aligned}$$

Using solution (22) for (14), the exact solution of the energy equation in the fixed frame satisfying the boundary conditions can be written as

$$\theta = -\frac{EcPr}{(1+\lambda_1)}\left[\frac{F_2^2}{2A^2}Y^2+\frac{1}{8A}(F_2^2+F_3^2)\cosh 2\left(\frac{Y}{\sqrt{A}}\right)\right.$$
$$\left.-\frac{Y^2}{4A^2}(F_2^2+F_3^2)+\frac{F_2F_3}{4A}\sinh 2\left(\frac{Y}{\sqrt{A}}\right)\right]+c_1Y+c_2, \quad (27)$$

where

$$c_1 = \frac{-1}{(h_1-h_2)}+\frac{EcPr}{(1+\lambda_1)(h_1-h_2)}$$
$$\cdot\left\{\frac{F_2^2}{2A^2}(h_1^2-h_2^2)-\frac{h_1^2-h_2^2)}{4A^2}(F_2^2+F_3^2)\right.$$
$$+\frac{1}{8A}(F_2^2+F_3^3)\left[\cosh 2\left(\frac{h_1}{\sqrt{A}}\right)-\cosh 2\left(\frac{h_2}{\sqrt{A}}\right)\right]$$
$$\left.+\frac{F_2F_3}{4A}\left[\sinh 2\left(\frac{h_1}{\sqrt{A}}\right)-\sinh 2\left(\frac{h_2}{\sqrt{A}}\right)\right]\right\},$$
$$c_2 = \frac{EcPr}{(1+\lambda_1)}\left\{\frac{F_2^2}{2A^2}h_1^2+\frac{F_2F_3}{4A}\sinh 2\left(\frac{h_1}{\sqrt{A}}\right)\right.$$
$$\left.-\frac{h_1^2}{4A^2}(F_2^2+F_3^2)+\frac{1}{8A}(F_2^2+F_3^2)\cosh 2\left(\frac{h_1}{\sqrt{A}}\right)\right\}-c_1h_1.$$

It is noticed that in the absence of heat transfer and slip parameter L the results of Kothandapani and Srinivas [1] can be recovered as a special case of our problem. Moreover, the results of Mishra and Rao [11] can be recovered if $\lambda_1 \to 0$, $L \to 0$ and in the absence of heat transfer.

5. Expression for Wave Shape

The non-dimensional expressions for the five considered wave forms are given by the following [31, 32]:

1. Sinusoidal wave

$$h(x) = 1+\phi\sin 2\pi x.$$

2. Multisinusoidal wave

$$h(x) = 1+\phi\sin 2\pi xn.$$

3. Square wave

$$h(x) = 1+\phi\left[\frac{4}{\pi}\sum_{m=1}^{\infty}\frac{(-1)^{m+1}}{(2m-1)}\cos[2(2m-1)\pi x]\right].$$

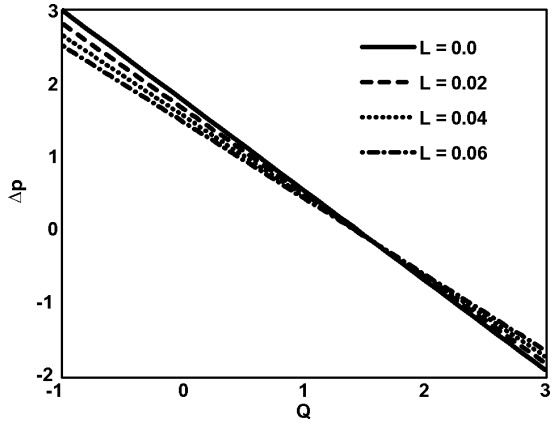

Fig. 2. Variation of Δp with Q for different values of L at $a = 0.7$, $b = 1.2$, $d = 2$, $M = 0.1$, $\phi = \frac{\pi}{6}$, $\lambda_1 = 0.4$.

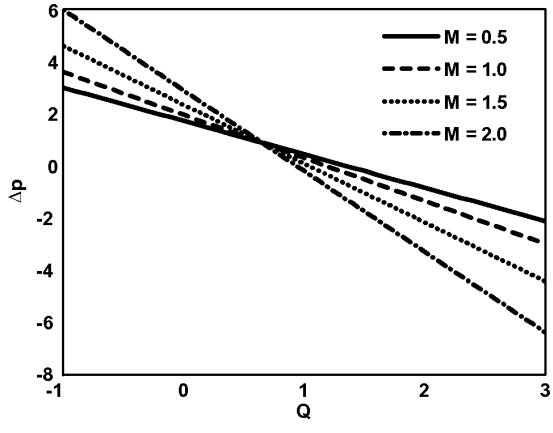

Fig. 3. Variation of Δp with Q for different values of M at $a = 0.7$, $d = 2$, $L = 0.02$, $\phi = \frac{\pi}{6}$, $\lambda_1 = 0.4$.

4. Triangular wave

$$h(x) = 1+\phi\left[\frac{8}{\pi^3}\sum_{m=1}^{\infty}\frac{(-1)^{m+1}}{(2m-1)^2}\sin[2(2m-1)\pi x]\right].$$

5. Trapezoidal wave

$$h(x) = 1+\phi\left[\frac{32}{\pi^2}\sum_{m=1}^{\infty}\frac{\sin[\frac{\pi}{8}(2m-1)]}{(2m-1)^2}\sin[2(2m-1)\pi x]\right].$$

6. Results and Discussion

In this section, the graphical results are displayed. The integration which appears to compute pressure rise Δp is calculated numerically using mathematics

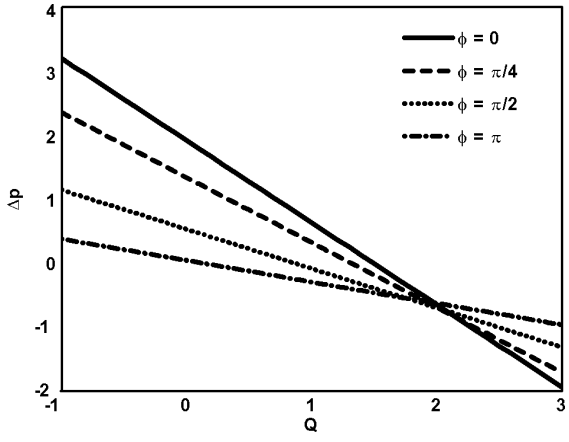

Fig. 4. Variation of Δp with Q for different values of ϕ at $a = 0.7$, $b = 1.2$, $d = 2$, $L = 0.02$, $M = 0.1$, $\lambda_1 = 0.4$.

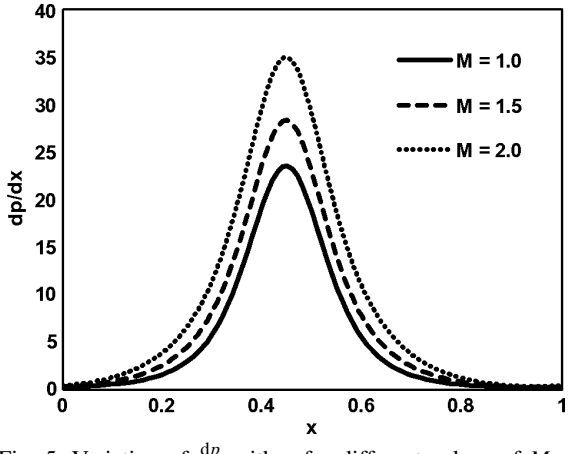

Fig. 5. Variation of $\frac{dp}{dx}$ with x for different values of M at $a = 0.7$, $b = 1.2$, $d = 2$, $L = 0.02$, $Q = -1$, $\phi = \frac{\pi}{6}$, $\lambda_1 = 0.4$.

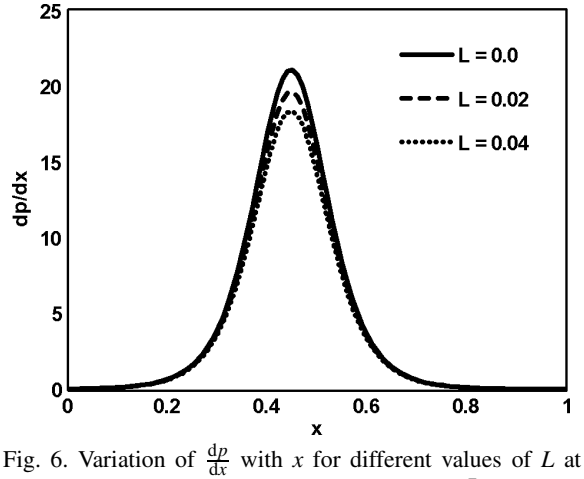

Fig. 6. Variation of $\frac{dp}{dx}$ with x for different values of L at $a = 0.7$, $b = 1.2$, $d = 2$, $M = 0.1$, $Q = -1$, $\phi = \frac{\pi}{6}$, $\lambda_1 = 0.4$.

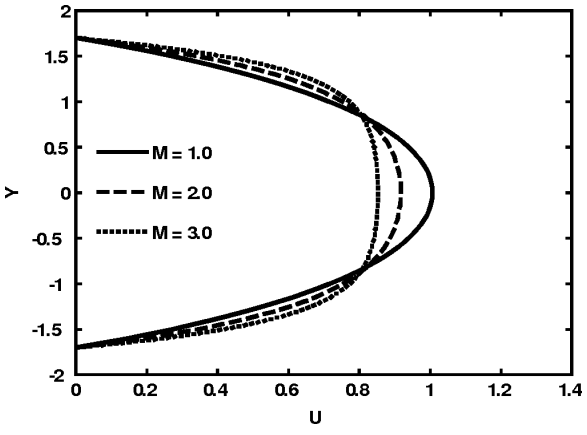

Fig. 7. Effect of M on velocity profiles at $a = 0.7$, $b = 0.7$, $d = 1$, $L = 0.02$, $X = 1$, $t = 1$, $\phi = 0$.

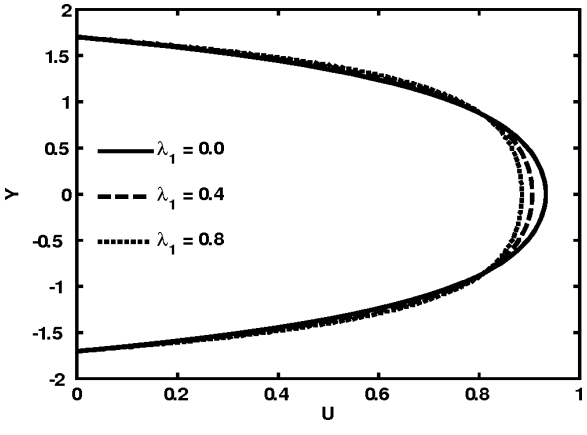

Fig. 8. Effect of λ_1 on velocity profiles at $a = 0.7$, $b = 0.7$, $d = 1$, $L = 0.02$, $X = 1$, $t = 1$, $\phi = 0$.

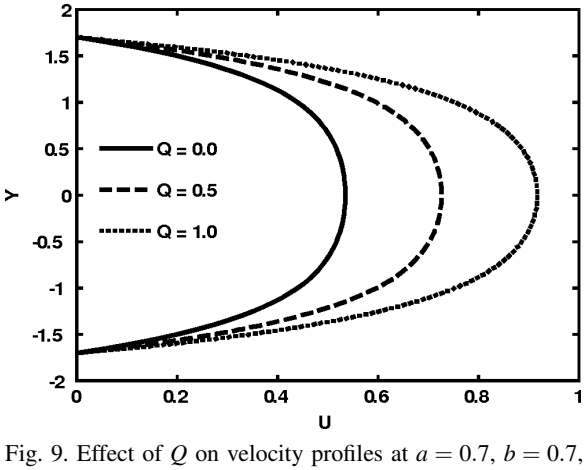

Fig. 9. Effect of Q on velocity profiles at $a = 0.7$, $b = 0.7$, $d = 1$, $L = 0.02$, $X = 1$, $t = 1$, $\phi = 0$.

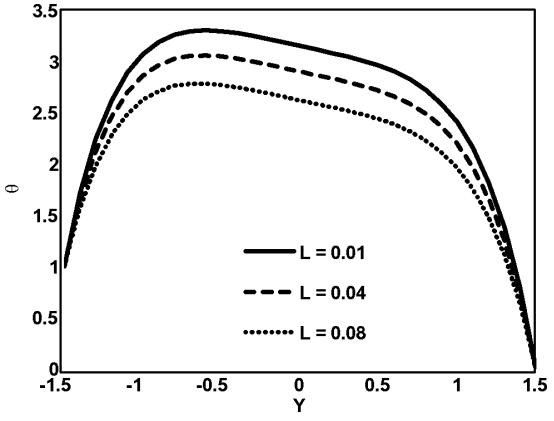

Fig. 10. Variation of θ with Y for different values of L at $a = 0.5, b = 1.2, d = 1.5, Q = -2, M = 0.1, \lambda_1 = 0.4, Er = 1, Pr = 1, X = 1, t = 1, \phi = \frac{\pi}{2}$.

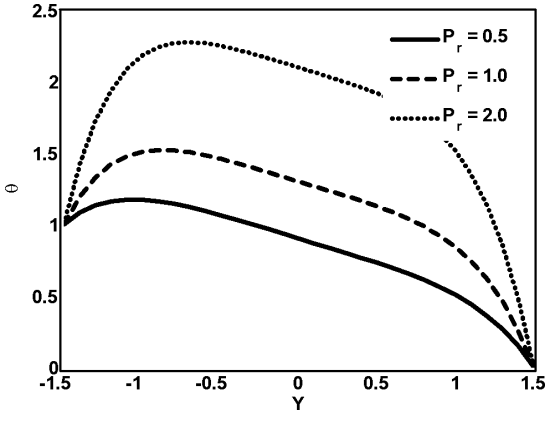

Fig. 11. Variation of θ with Y for different values of Pr at $a = 0.5, b = 1.2, d = 1.5, Q = -1, M = 0.1, \lambda_1 = 0.4, Er = 1, L = 0.02, X = 1, t = 1, \phi = \frac{\pi}{2}$.

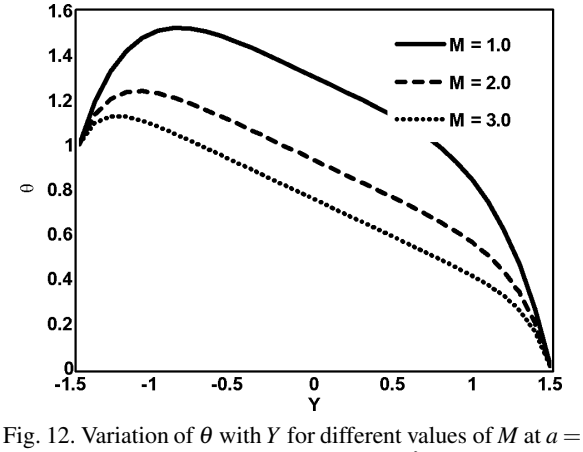

Fig. 12. Variation of θ with Y for different values of M at $a = 0.5, b = 1.2, d = 1.5, Q = -2, L = 0.02, \lambda_1 = 0.4, Er = 1, Pr = 1, X = 1, t = 1, \phi = \frac{\pi}{2}$. Fig. 12.

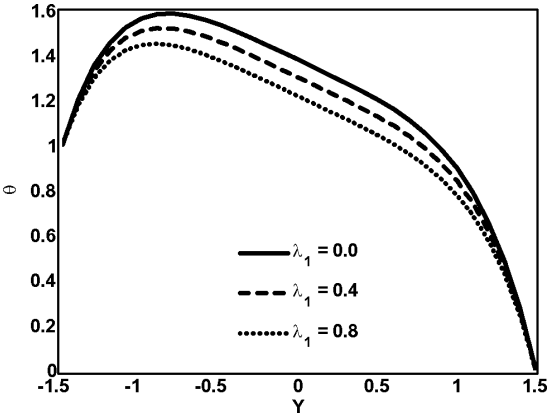

Fig. 13. Variation of θ with Y for different values of λ_1 at $a = 0.5, b = 1.2, d = 1.5, Q = -2, M = 0.1, L = 0.02, Er = 1, Pr = 1, X = 1, t = 1, \phi = \frac{\pi}{2}$.

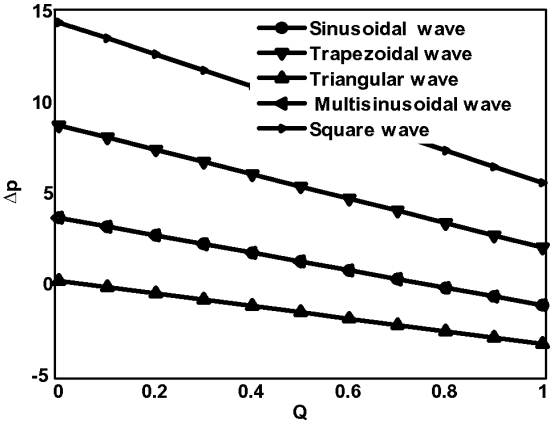

Fig. 14. Variation of Δp with Q for different wave form at $a = 0.7, b = 1.2, d = 2, M = 3, L = 0.02, \lambda_1 = 2, \phi = \frac{\pi}{6}$.

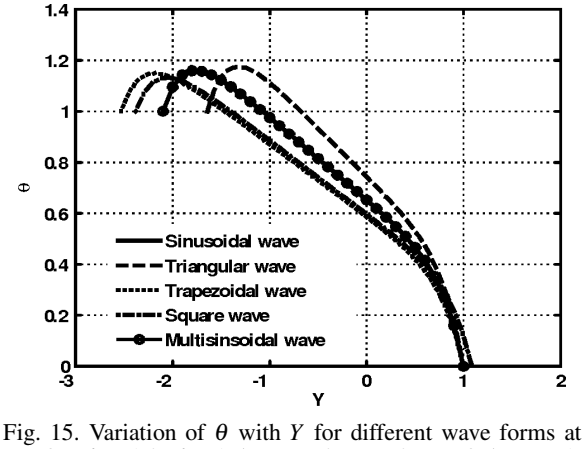

Fig. 15. Variation of θ with Y for different wave forms at $a = 0.7, b = 1.2, d = 1.5, Q = -2, M = 2, L = 0.5, Er = 1, Pr = 1, \phi = \frac{\pi}{6}, X = 1, t = 1, \lambda_1 = 0.4$.

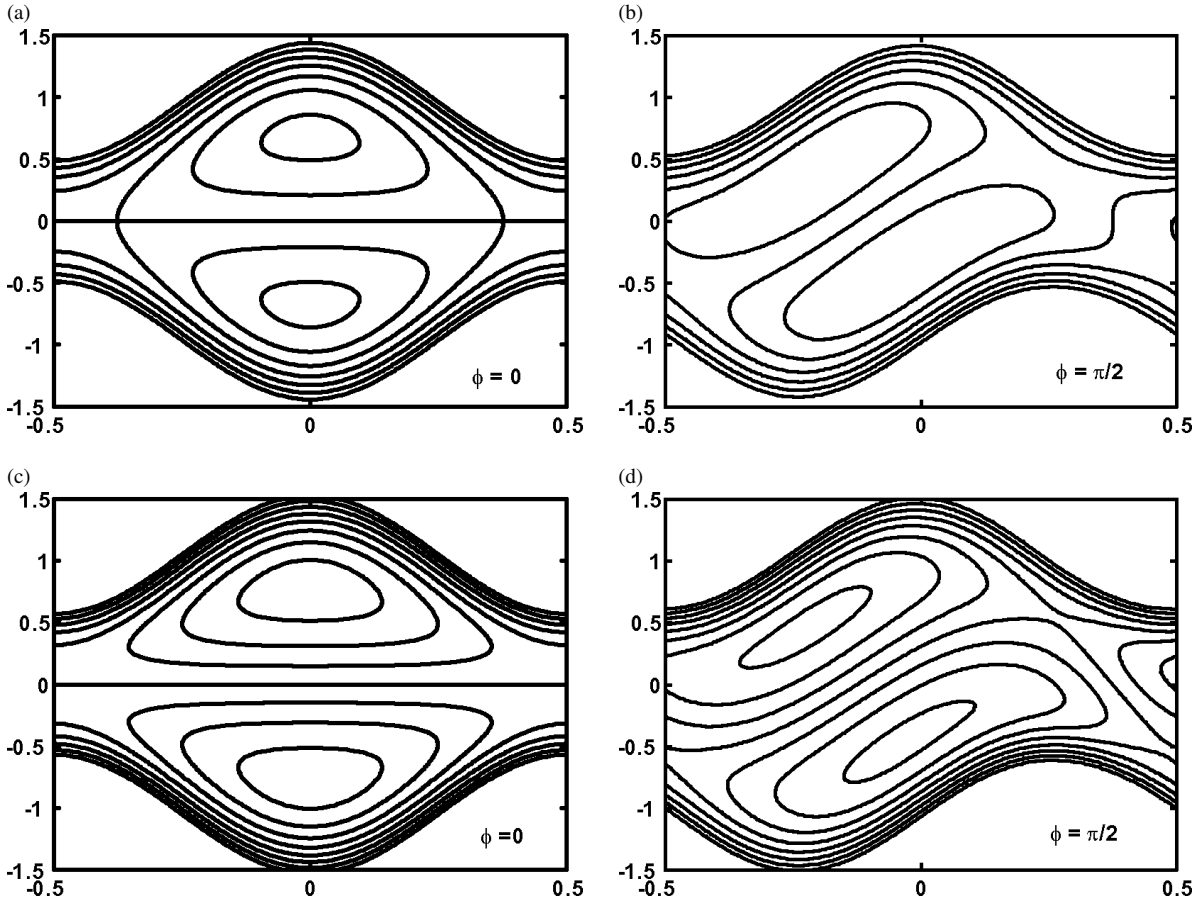

Fig. 16. Stream lines for three different values of L. (a) and (b) for $L = 0.01$, (c) and (d) for $L = 0.03$. The other parameters are chosen as $a = 0.5$, $b = 0.5$, $d = 1.0$, $Q = 1.45$, $\lambda_1 = 0.1$, $M = 1$.

software. The pressure rise Δp for different values of slip parameter L, magnetic parameter M, and amplitude ratio ϕ are plotted in Figures 2 to 4. Figure 2 illustrate the pressure rise for different values of L. It is shown that Δp decreases for small values of Q with the increase in L, however, Δp increases for large values of Q with the increase in L. Thus, we say that Δp and Q has inversely linear relation between each other. Figure 3 represents the variation of Δp with Q for different values of M. It is observed that the pressure rise increases with the increase in M for small Q whereas for large Q, Δp decreases with the increase in M. The effects of the amplitude ratio ϕ on the pressure rise are shown in Figure 4. It is observed that for $Q \in [-1,2]$, the pressure rise decreases with the increase in ϕ, whereas for $Q \in [2,3]$, the pressure rise increases. The pressure gradient for different values of M and L against x is plotted in Figures 5 and 6. It is depicted from these figures that for $x \in [0,0.2]$ and $x \in [0.8,1]$ the pressure gradient is small, i. e., the flow can easily pass, while in the region $x \in [0.2,0.8]$, the pressure gradient increases with the increase in M and decreases with the increase in L and much pressure gradient is required to maintain the flux to pass. The velocity field for several values of M, λ_1, and Q are shown in Figures 7 to 9. It is seen from Figures 7 and 8 that for $Y \in [-1.65,-1]$ and $[1,1.65]$, the velocity field show a slight increase with an increase in M, while for $Y \in [-1,1]$ with the increase in M and λ_1, the velocity decreases and the maximum value of velocity is at the center of the channel. The velocity profile for different values of Q is shown in Figure 9. It is observed that the velocity profile increases with the increase in Q. The temperature profile for several values of L, Pr, M, and λ_1 are shown in Figures 10 to 13. It is observed that the temperature field decreases with

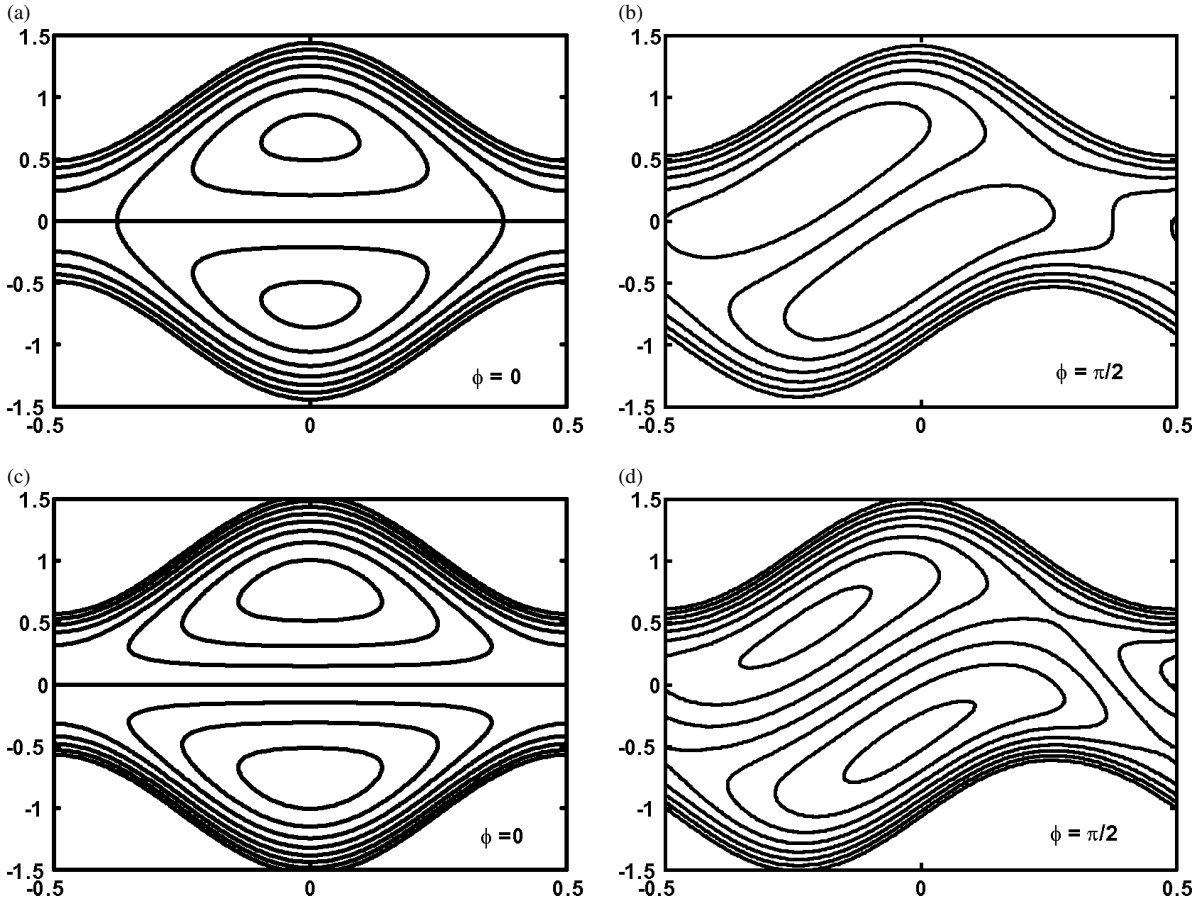

Fig. 17. Stream lines for three different values of Q. (a) and (b) for $Q = 1.8$, (c) and (d) for $Q = 2.0$. The other parameters are chosen as $a = 0.5$, $b = 0.5$, $d = 1.0$, $L = 0.02$, $\lambda_1 = 0.2$, $M = 1$.

the increase of L, M, and λ_1, while it increases with the increase in Pr. The pressure rise Δp for different types of waves is presented in Figure 14. It is observed that Δp in a trapezoidal wave is greater than in a sinusoidal wave which is greater than in a triangular wave. The temperature field for different wave forms are presented in Figure 15. It is observed that the temperature field for a sinusoidal wave is greater than for a trapezoidal wave and the temperature field for a triangular wave is greater than for a sinusoidal wave.

Table 1. Comparison of pressure rise with volume flow rate for fixed $a = 0.7$, $b = 1.2$, $d = 2$, $M = 0.1$, $\phi = \frac{\pi}{6}$, $\lambda_1 = 0.4$.

Q	Kothandapani and Srinivas [1] when $L = 0$	Present work when $L = 0.02$
−1	2.98239	2.80332
−0.5	2.36653	2.22225
0	1.75066	1.64118
0.5	1.13479	1.06011
1	0.518927	0.479047
1.5	−0.09694	−0.10202
2	−0.712807	−0.683087
2.5	−1.32867	−1.26415
3	−1.94454	−1.84522

6.1. Trapping Phenomena

Another interesting phenomena in peristaltic motion is trapping. It is basically the formation of an internally circulating bolus of fluid by closed stream lines. This trapped bolus pushed a head along peristaltic waves. Figures 16 to 18 illustrate the stream lines for different values of L, Q, and M for both symmetric and asymmetric channel. It is observed from the figures that for a symmetric channel the trapping bolus is symmetric about the centre line of the channel (see panels (a) and (c)), while in case of an asymmetric channel the

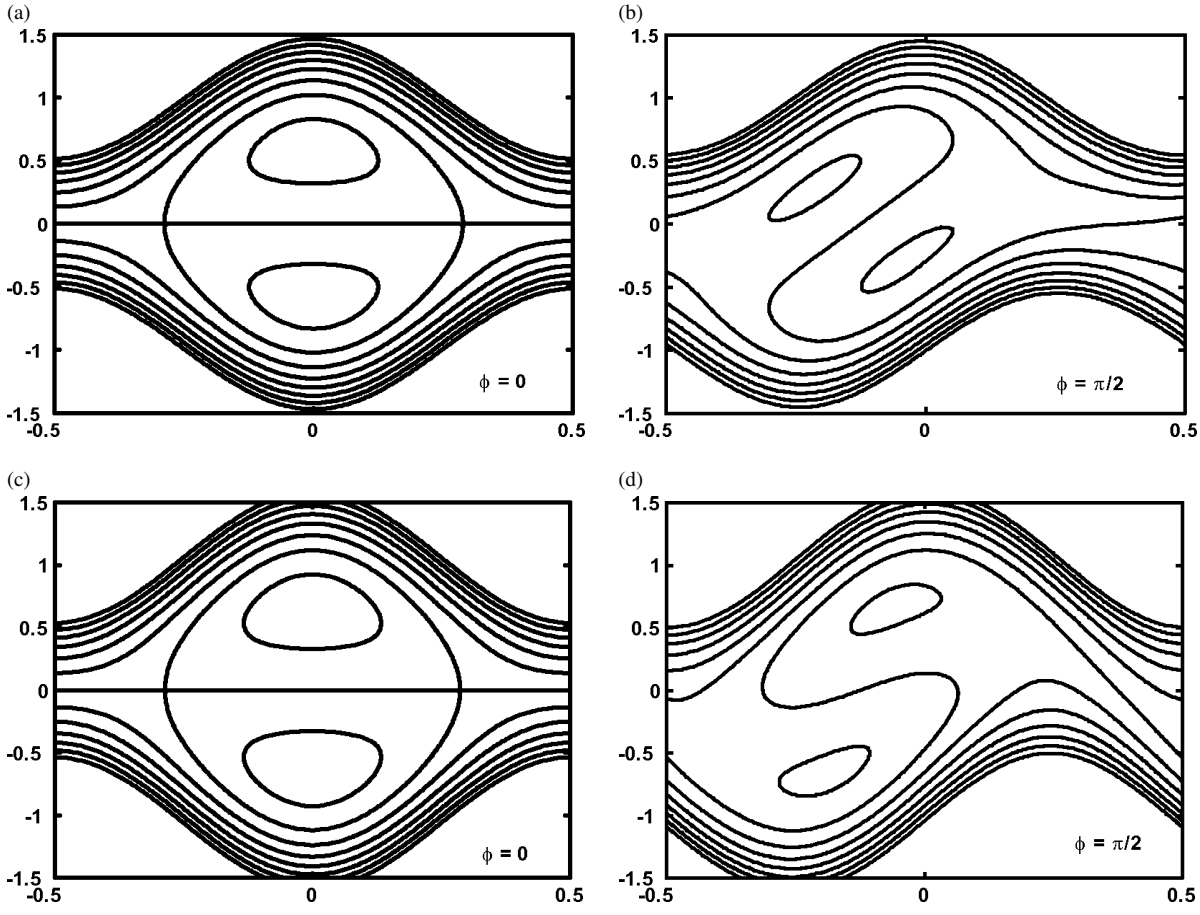

Fig. 18. Stream lines for three different values of M. (a) and (b) for $M = 1.0$, (c) and (d) for $M = 1.1$. The other parameters are chosen as $a = 0.5$, $b = 0.5$, $d = 1.0$, $L = 0.02$, $\lambda_1 = 0.2$, $Q = 1.45$.

Table 2. Comparison of velocity profile for fixed $a = 0.7$, $b = 0.7$, $d = 1$, $X = 1$, $t = 1$, $\phi = 0$.

Y	Kothandapani and Srinivas [1] when $L = 0$	Present work when $L = 0.02$
−1.7	0	0
−1.3	0.5619	0.574951
−0.9	0.794255	0.786245
−0.5	0.887231	0.870794
−0.1	0.916923	0.897794
0.1	0.916923	0.897794
0.5	0.887231	0.870794
0.9	0.794255	0.786245
1.3	0.5619	0.574951
1.7	0	0

bolus tends to shift towards the left side of the channel due to the phase angle (see panels (b) and (d)). Figure 16 shows the stream lines for different values of slip parameter L. It is observed that with the increase in L the size of the trapping bolus decreases. Moreover, it is also observed that the size of the trapping bolus is small in an asymmetric channel as compared with the symmetric channel. From Figure 17 we learn that with the increase in Q, the size and the number of the trapped bolus increases. The size of the trapped bolus increases with the increase in M (Fig. 18). Stream lines for different wave forms are presented in Figure 19. It is observed that the size of the trapped bolus is smaller in case of a triangular wave when compared with other wave forms.

Table 1 and 2 show the comparison of the present solution with those available in the literature when some of the parameters are replaced to be zero in our problem.

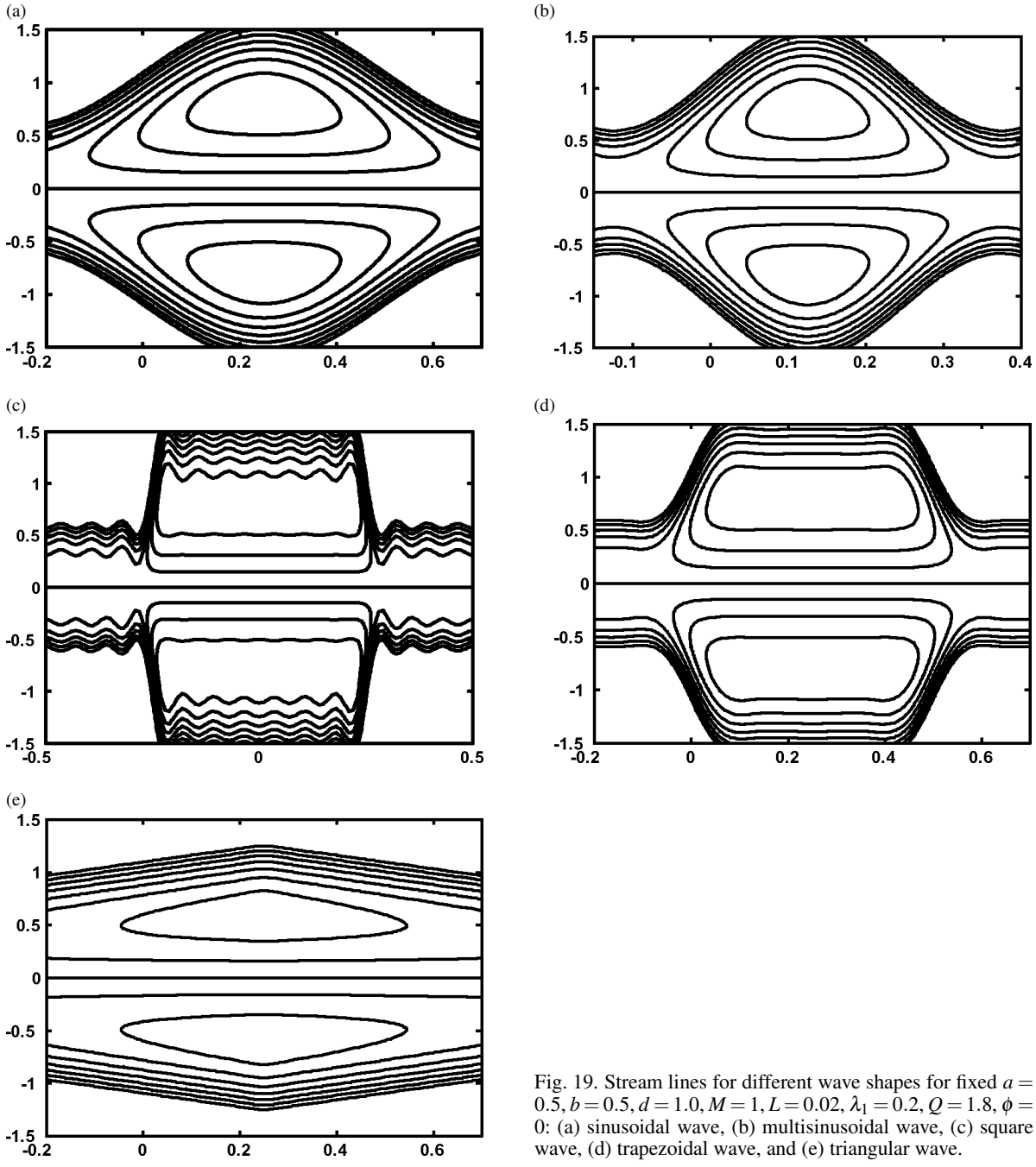

Fig. 19. Stream lines for different wave shapes for fixed $a = 0.5, b = 0.5, d = 1.0, M = 1, L = 0.02, \lambda_1 = 0.2, Q = 1.8, \phi = 0$: (a) sinusoidal wave, (b) multisinusoidal wave, (c) square wave, (d) trapezoidal wave, and (e) triangular wave.

[1] M. Kothandapani and S. Srinivas, Int. J. Nonlinear Mech. **43**, 915 (2008).
[2] T. Hayat, N. Ali, S. Asghar, and A. M. Siddiqui, Appl. Math. Comput. **182**, 359 (2006).
[3] A. H. Abd El-Naby and A. E. M. El-Misiery, Appl. Math. Comput. **128**, 19 (2002).
[4] T. Hayat and N. Ali, Phys. A **370**, 225 (2006).
[5] Kh. S. Mekheimer, Arab. J. Sci. Eng. **28**, 183 (2003).
[6] A. H. Shapiro, M. Y. Jaffrin, and S. L. Weinberg, J. Fluid Mech. **37**, 799 (1969).
[7] M. Ealshahed and M. H. Haroun, Math. Prob. Eng. **6**, 663 (2005).

[8] M. H. Haroun, Commun. Nonlinear Sci. Numer. Simul. **12**, 1464 (2007).
[9] M. H. Haroun, Comput. Material Sci. **39**, 324 (2007).
[10] A. El Hakeem, A. El Naby, A. E. M. El Misiery, and I. I. El Shamy, J. Phys. A: Math. Gen. **36**, 8535 (2003).
[11] M. Mishra and A. R. Rao, Z. Angew. Math. Phys. **53**, 532 (2003).
[12] M. Y. Jaffrin and A. H. Shaprio, Ann. Rev. Fluid Mech. **3**, 13 (1971).
[13] E. F. Elshehawey, N. T. Eladabe, E. M. Elghazy, and A. Ebaid, Appl. Math. Comput. **182**, 140 (2006).
[14] T. Hayat, Q. Hussain, and N. Ali, Phys. A **387**, 3399 (2008).
[15] T. Hayat, N. Ahmad, and N. Ali, Commun. Nonlinear Sci. Numer. Simul. **13**, 1581 (2008).
[16] Kh. S. Mekheimer and Y. Abdelmaboud, Phys. Lett. A **372**, 1657 (2008).
[17] R. C. Eberhart and A. Shitzer, Heat Transfer in Medicine and Biology, 1st edn., Springer, Berlin 1985.
[18] G. Radhakrishnamacharya and Ch. Srinivasulu, C. R. Mecanique **335**, 369 (2007).
[19] G. Radhakrishnamacharya and V. Radhakrishna Murthy, Def. Sci. J. **43**, 275 (1993).
[20] S. Srinivas and M. Kothandapani, Int. Commun. Heat Mass Transf. **35**, 514 (2008).
[21] S. Srinivas and R. Gayathri, Appl. Math. Comput. **215**, 185 (2009).
[22] Kh. S. Mekheimer, S. Z. A Husseny, and Y. Abd Elmaboud, Numer. Method. Partial Diff. Eqs. doi10.1002/num.20451.
[23] S. Srinivas and M. Kothandapani, Appl. Math. Comput. **213**, 179 (2009).
[24] N. T. Eldabe, E. M. Elghazy, and A. Ebaid, Phys. Lett. A **363**, 257 (2007).
[25] G. Adomian, Solving frontier problems of physics, The decomposition method. Kluwer Acad. Press, Boston 1994.
[26] A. M. Wazwaz, Appl. Math. Comput. **61**, 543 (2005).
[27] G. Adomian, Nonlinear Stochastic Operator Equations. Academic Press Orlando, FL 1986.
[28] A. M. Wazwaz, Appl. Math. Comput. **128**, 47 (2002).
[29] A. M. Wazawaz, Partial differential equations, Method and Applications. Balkema Publishers, The Netherlands 2002.
[30] A. M. Wazawaz, Appl Math. Comput. **123**, 109 (2001).
[31] T. Hayat, N. Ali, and Z. Abbas, Phys. Lett. A **370**, 331 (2007).
[32] P. Hariharan, V. Seshadrib, and R. K. Banerjee, Math. Comput. Modelling **48**, 998 (2008).